A Novel Green Synthesis of Zinc Sulfide Nano-Adsorbents Using Artemisia Herba Alba Plant Extract for Adsorption and Photocatalysis of Methylene Blue Dye

Sabri Ouni, Naim Bel Haj Mohamed, Mohamed Haouari, Abdelhamid Elaissari, Abdelhamid Errachid, Nicole Jaffrezic-Renault

A novel green synthesis of zinc sulfide nano-adsorbents using *Artemisia Herba Alba* plant extract for adsorption and photocatalysis of methylene blue dye

Sabri Ouni [a,b], Naim Bel Haj Mohamed [c], Mohamed Haouari [b], Abdelhamid Elaissari [a], Abdelhamid Errachid [a], and Nicole Jaffrezic-Renault [a*]

[a] Institute of Analytical Sciences, University of Lyon, 69100 Villeurbanne, France

[b] Laboratory of Advanced Materials and Interfaces (LIMA), University of Monastir, Faculty of Sciences of Monastir, Monastir-Tunisia

[c] Faculty of Sciences, Laboratory of Spectroscopic Characterization and Optical Materials (LaSCOM), University of Sfax, B.P. 1171, 3000 Sfax, Tunisia

**Corresponding authors E-mail: nicole.jaffrezic@univ-lyon1.fr*

Abstract

We report a facile and green route for a new synthesis of sulfide nanoparticles (ZnS NPs) using *Artemisia Herba Alba* (AHA) plant extract for efficient adsorption/photodegradation of methylene blue dye (MB). Results exhibited a blue shift in the absorbance band and higher energy band gap values than bulk ZnS materials, which was due to the quantum confinement effect. X-ray diffraction confirmed the formation of the cubic phase of ZnS-AHA nanocrystals with a calculated average size of 4 nm. Green synthesized ZnS NPs show enhanced adsorption efficiency toward MB from contaminated water. ZnS-AHA NPs showed a specific surface area of 36.82 cm^2 g^{-1} and an adsorption capacity of 31.17 mg g^{-1} for MB. The Langmuir-Freundlich model modeled adsorption data. The photocatalytic degradation performance of the green nanoparticles under sunlight irradiation showed a remarkable dye degradation rate of 94.09% in 180 min. In summary, this eco-friendly NPs is a highly promising material to be used in wastewater treatment for the removal of organic compounds.

Keywords: Green synthesis; *Artemisia Herba Alba;* nanoparticles; Adsorption; Statistical physics modeling; Photocatalysis; Methylene Blue.

1. Introduction

Finding a way to treat wastewater that is safe for living things, cheap, and effective remains a challenge for humanity. Due to the widespread industrialization of the world, the situation is much worse than it used to be. This has caused many serious problems for our environment,

such as the pollution of water by dumping pollutants like organic dyes into rivers, lakes, streams, and ponds without first cleaning them [1]. These toxic chemicals are difficult to biodegrade, and they remain in soil and water for years, which causes serious health dangers to living organisms and also reduces soil fertility as the photosynthetic activity of aquatic plants results in the development of anoxic conditions for aquatic flora [2,3]. To protect the environment, it is important to limit these toxic wastes as much as possible by coming up with an effective way to treat wastewater before it is released.

In recent decades, numerous chemical, physical and biological methods were proposed for wastewater treatment, including membrane-based processes, ultrafiltration, and reverse osmosis [4]. Nevertheless, dyes reveal high solubility in water, which makes them difficult to eliminate by such traditional procedures [5,6]. Among the current techniques, the so-called advanced oxidation processes (AOP) have emerged as one of the most powerful means for dye degradation. Some AOPs methods such as ozonation have reached a level of development at an industrial scale, while others are in full development in the research field [7]. These processes allow the elimination of organic pollutants at atmospheric pressure and ambient temperature using extremely oxidizing and reactive radical species able to degrade a wide variety of molecules, and they may eventually lead to the complete mineralization of the pollutants. Heterogeneous solar photocatalysis is one of the most studied, environmentally compatible, and efficient processes for degrading many non-biodegradable pollutants using solar resources [8]. A photocatalyst is used in this process to start a chemical reaction when it is exposed to sunlight. In this process, the photocatalyst is typically a semiconductor material, which absorbs light and generates electron-hole pairs that can react with water and other organic molecules.

Among the different semiconductors, zinc sulfide (ZnS) has been the focus of much attention in view of its low cost, abundance,good stability, non-toxicity, and high optical absorption in the visible and ultraviolet ranges [9]. Indeed, ZnS nanoparticles (NPs) are synthesized through various methods, including chemical precipitation, solvothermal synthesis, and hydrothermal synthesis [10]. These methods allow for precise control over the size, shape, and properties of the nanoparticles. ZnS NPs have potential applications in various fields, including as a material for optoelectronic devices, such as solar cells and light-emitting diodes (LEDs), and as a photocatalyst for water splitting and pollutant degradation [11]. They have also been studied for their potential in biomedical applications, such as imaging and drug delivery.

Traditional ways of making NPs, on the other hand, often involve using toxic chemicals and solvents, which can be bad for the environment. Therefore, there is a growing interest in developing environmentally friendly methods for the biosynthesis of NPs. One such approach is the use of biological agents, such as microorganisms, plants, and enzymes, for the synthesis of NPs. These agents can reduce metal ions and generate NPs through a process known as bio-reduction. For example, nanoparticles can be synthesized using biological substances such as plants, algae [12], bacteria [13], fungi, and viruses [14], which is defined as a novel, simple, fast, economic and ecological alternative.

Currently, there is an increasing interest in the green chemistry method for synthesizing zinc sulfide [15,16]. Rajabi et al. used the leaf extract of *F. Johannis*, and they obtained spherical and semi-spherical nanoparticles of ZnS [17]. On the other side, Kannan et al. reported on the synthesis of ZnS nanoparticles with a spherical form and an average size between 5 and 20 nm using *Acalypha indica* and *Tridax procumbens* [18]. Plant extracts have several benefits, such as safe handling and non-toxicity. Also, they can act as both reducing and stabilizing agents for nanoparticles, allowing the simple fabrication of large amounts of nanoparticles [19].

To our knowledge, the use of an aqueous extract of *Artemisia Herba Alba* (AHA) for the green synthesis of ZnS nanoparticles has not been reported. In this context, *Artemisia Herba Alba* is a species of aromatic plant that belongs to the family Asteraceae. It is commonly known as desert wormwood, or also known in Tunisia as 'Chih', and is native to North Africa and the Middle East [20]. This plant has a woody stem and grows up to 60 cm tall. The leaves are silver-gray in color, hairy, and divided into small lobes. The plant produces small, yellow flowers in the summer. The AHA plant has been used in traditional medicine for a variety of purposes, including the treatment of digestive disorders, respiratory problems, and skin conditions. It is also used as a natural insect repellent [20]. Recent studies have shown that the plant contains compounds with potential therapeutic properties, including antioxidant, anti-inflammatory, and antimicrobial effects. However, more research is needed to fully understand the plant's potential benefits [21]. This desert wormwood has more than 160 individual components, including many essential oils, terpenoids, flavonoids, luteolin and flavones [22]. These phyto-bioactive constituents, which are present in the aqueous extract of AHA, play an essential role in capping and stabilizing the biosynthesized nanoparticles.

In the present study, the authors attention is focused on preparing a new green synthesis of ZnS colloidal nanoparticles using *Artemisia Herba Aba* (ZnS-AHA) plant extract by chemical route

and subjecting them to several experimental techniques to explore their applications in the adsorption/photodegradation of a cationic thiazine dye, methylene blue (MB). MB is a cationic dye commonly used in industries such as textiles, paper, and printing [23]. The adsorption of MB on green-capped ZnS NPs was studied at different operating conditions. The effect of temperature on the adsorption process was analyzed. MB degradation with ZnS-AHA nanocatalysts was assessed at operating conditions under sunlight irradiation.

2. Experimental

Details regarding experimental and Artemisia Herba Alba extraction should be found in the supplementary information.

3. Results and discussion

3.1. ZnS-AHA nanoparticules characterization

The compositions of biologically active compounds in *A. annua* extract utilized for ZnS-AHA NPs preparation were determined by FTIR analysis. The FTIR spectrum is presented in **Fig.S2**. The FTIR analysis exhibited a major vibrational band at 540 cm^{-1}, which is associated with the Zn-S stretching vibrations [24,25]. The absorption peak was observed at 3319 cm^{-1} which is due to the alcohol/phenol group (-OH) stretching vibration [26]. The peak at 2978 cm^{-1} is probably ascribed to C-H alkane stretching, while the band at 2893 cm^{-1} could be assigned to the C-H stretching of branched alkenes, particularly from AHA extract [27,28]. The peaks of FT-IR analysis were evidence that the ZnS-AHA NPs were alleviated with the major phytoconstituents of *Artemisia Herba Alba* extract utilized for ZnS NPs fabrication.

The crystal structures of the as-synthesized ZnS nanoparticles prepared using AHA were determined by X-ray diffraction analysis; see Fig. **S3**. XRD confirmed the formation of the cubic phase of ZnS-AHA nanocrystals with a calculated average size of 4 nm. The sharp and narrow peaks implied that the ZnS-AHA NPs were highly crystallized [29]. The smaller size of the ZnS crystallites encapsulated by AHA extract is most likely due to the strong interaction of AHA molecules with ZnS nanocrystals [30].

The size distribution and morphology of the synthesized ZnS-AHA NPs were imaged using HR-TEM. The ZnS-AHA NPs microscopic analysis with TEM was presented in **Fig.S4a**. In general, the TEM images have revealed the sphere's spherical shape, with diameters in the range of 4 nm. These results are in good agreement with the XRD results. The d-spacing determined from the digital micrograph for ZnS is 0.30 nm, which is close to the spacing of the (111) diffraction plane of the cubic phase [8]. NPs elemental composition was determined by EDX (**Fig.**

S4b). Zn and S are the major elemental components. The presence of C is related to the TEM grid, and other peaks, Si and P, are probably due to residues coming from the synthesis and the grid.

Fig. S5 shows the optical absorption spectra of the ZnS NPs that were spread out in water. A broad, strong absorption band located at 325 nm confirms the single-dispersed nature of ZnS-AHA NPs distribution [31]. The estimated band gap energy for the green ZnS using the Tauc relation [32] is 3.70 eV, which indicates that the gap energy of ZnS-AHA NPs shifts towards the blue compared to that of bulk ZnS (Eg=3.6eV).

The photoluminescence spectra of the synthetized nanoparticles dispersed in water were recorded in (**Fig. S6**). An intense and wide band centered at 450 nm dominates the spectrum, which was attributed to recombination between electrons and holes at the edges of the conduction and valence bands, respectively [33,34]. The FWHM of the main emission band is equal to 62 nm, which is related to the size dispersion of the ZnS-AHA NPs.

In the extra information, you can find more information about how our samples are described.

3.2. Adsorption study of MB on AHA capped ZnS nanoparticles

In general, studies show that the amount of dye that can be removed increases significantly as the adsorbent's efficiency goes up [35]. The effect of the mass of the AHA-capped ZnS NPs on the MB adsorption is revealed in **Fig. 1.** The amount of the nanoadsorbents is varied from 0.1 to 2 g, the concentration of dye being 10 mg/l at pH = 7, the temperature being 298 K, and the contact time being 120 min. This figure exhibits that the removal of dye increases as the amount of the adsorbent increases. This is easily understandable, as the increase in adsorbent mass increases the available surface area and therefore the number of adsorption sites available [36] and consequently increases the amount of dye adsorbed. The dye removal reached approximately 95.91% using 1 g of green AHA-capped NPs, which is related to a large number of adsorption sites. On further addition of adsorbents, a decrease in the adsorption efficiency of nano-adsorbents was observed. This is explained by the fact that the accessibility of adsorbent active sites with higher energy decreases, and only the active sites with lower energy are available to be occupied [37]. Therefore, the optimum amount for dye removal was chosen to be 1 g of ZnS-AHA NPs.

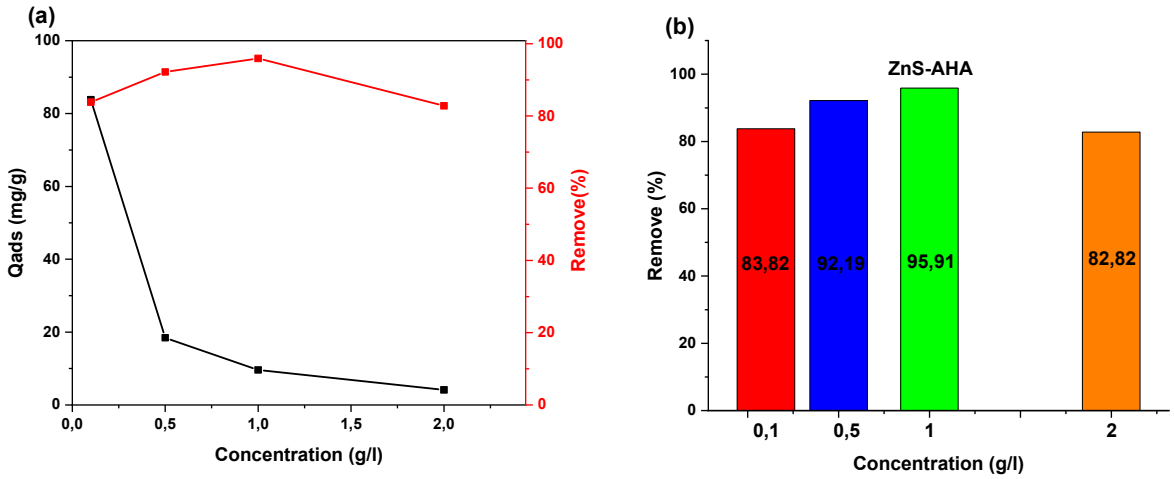

Fig.1: (a) Effect of ZnS-AHA mass on the MB adsorption and (b) Efficiency of MB adsorption.

The pH of the solutions is also an important factor that influences the capacity of the adsorbent by influencing the surface charge of the nanoparticles [24]. The effect of the solution pH on the dye adsorption was studied from 5 to 9, when keeping the dye concentration equal to 10 mg/l, the adsorbent quantity equal to 1 g and the temperature at 300 K. As shown in **Fig. 2**, the percentage of dye removal increased gradually from 70.55 to 95.91% when pH varies from 3 to 7; this is due to the electrostatic interactions between the positively charged dye molecules and the negatively charged adsorbents [24]. On the other hand, a decreasing trend in the dye removal efficiency was observed with a further increase in pH to 9. The pH value equal to 7 was fixed as the optimum pH for MB dye experiments.

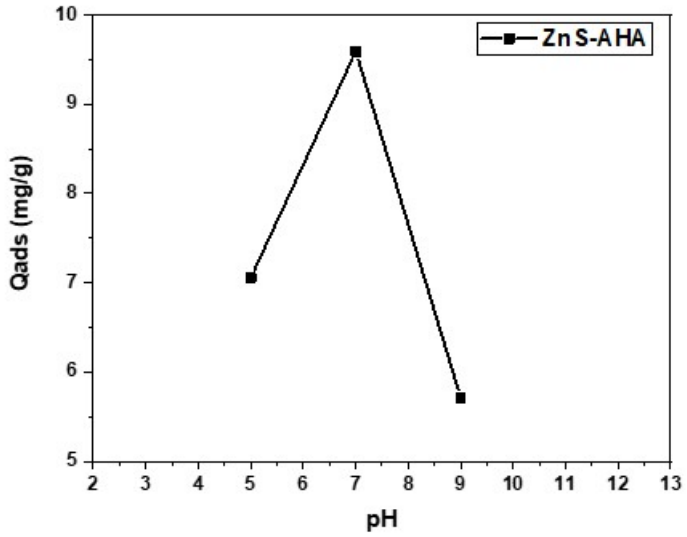

Fig.2: Effect of pH on the adsorption of MB by AHA-capped ZnS NPs.

Over time, adsorption was studied to find out how much dye was taken up at different times. Equilibration time is also an important economic factor for the water treatment of polluted systems [38]. The results of the kinetic adsorption study of MB on green capped ZnS NPs are presented in **Fig. 3**. The dye adsorption process on the AHA-capped ZnS nanoparticles was fast for the first 5 min, then continued at a slower rate for 10–30 min, reaching equilibrium after approximately 45 min of the experiment. The experimental kinetics showed that using an AHA ligand increased the MB adsorption capacity. This can be explained by the small size of the robust adsorbents, which have a large surface-to-volume ratio and provide more sites on the surface. Hence, we could deduce that the new green synthesis has a progressive impact on the adsorption process with the improvement of the adsorption efficiency in addition to the eco-friendly criteria. The effect of the initial dye concentration depends on the immediate relation between the dye concentration and the available nano-adsorbent surface sites, as shown in **Fig. 4**. The ability of the adsorbent goes up as the initial dye concentration goes up. This may be because the driving force for mass transfer is high when the initial dye concentration is high [39]. Experimental data exhibit an outstanding MB adsorption capacity on AHA-capped ZnS NPs, which varied from 9.54 to 29.92 mg/g when the dye concentration is raised from 10 to 50 mg/L, and it was assumed that *Artemisia Herba Alba* plant extract enhanced the adsorption process. However, another parameter is the temperature, which influences the adsorption capacity of the adsorbent. A decrease in the adsorption process has been noted, and the results are

given in **Fig. 5**. A decline of adsorption capacity with an increase in temperature demonstrates that the adsorption is an exothermic process. This may be attributed to the decline in the adsorptive forces between the dye species and the active sites on the adsorbent surface with a rise in temperature [40]

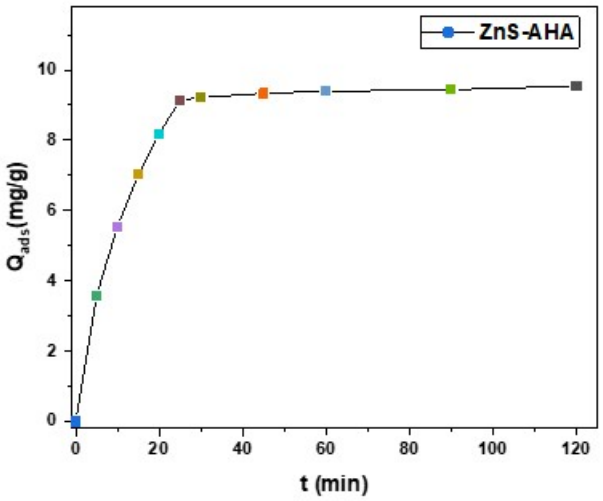

Fig. 3: kinetic adsorption study of MB on green capped ZnS NPs.

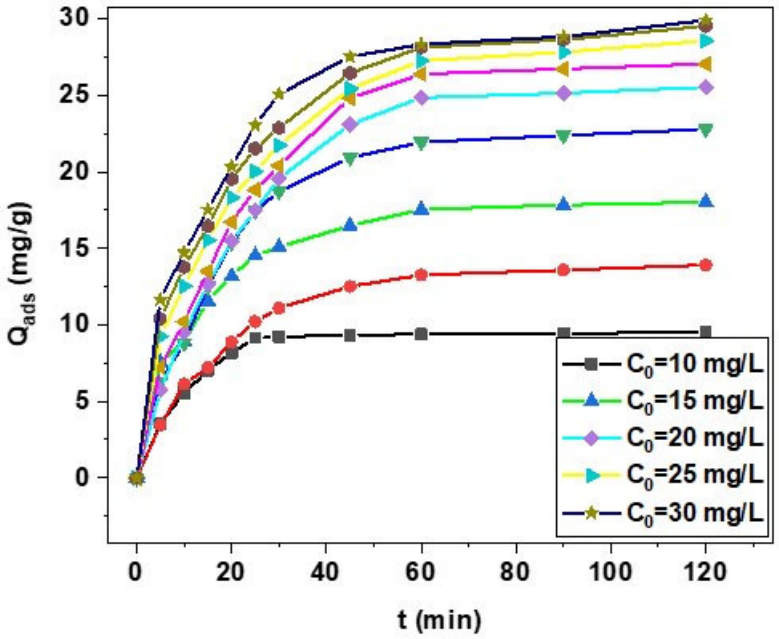

Fig.4: Effect of initial dye concentration on the adsorption capacity AHA-capped ZnS NPs.

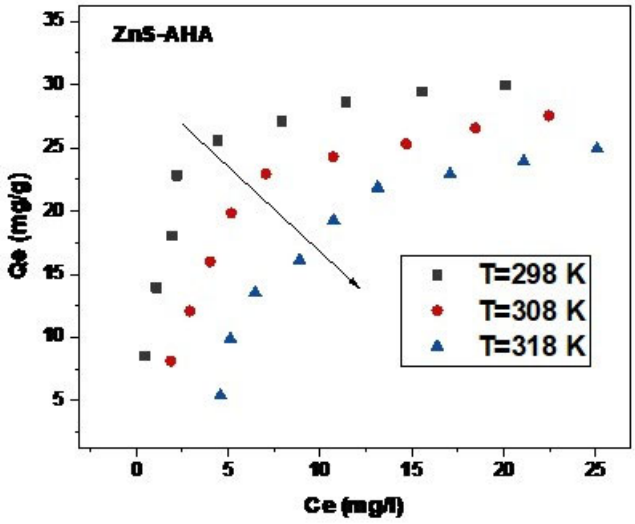

Fig. 5: Effect of Temperature on the adsorption of MB onto AHA-capped ZnS NPs.

3.2.1. Adsorption kinetics

The kinetics studies on MB adsorption were conducted at 298 K. The pseudo-first-order (PFO) and the pseudo-second-order (PSO) models were applied to evaluate the MB adsorption kinetic data. The PFO kinetic model has been widely employed to predict the dye adsorption kinetics, which is given by the next formula [41] :

$$q\ (t) = q_e\ (1\text{-}exp(\text{-}K_1 t) \qquad (1)$$

Where q(t) and q_e represent the amount of dye adsorbed (mg/g) at any time t and equilibrium, respectively, K_1 is the corresponding PFO adsorption rate constant (min^{-1}).

On the other side, the PSO kinetic model predicts that the rate-limiting step is chemisorption and this model is valid over the whole range of adsorption. The PSO kinetic rate equation is defined as follows [41] :

$$q(t) = \frac{q_e^2 k_2 t}{1+q_e K_2 t} \qquad (2)$$

Where K_2 (mg/g min) is the corresponding PSO rate adsorption constant. The best model for the adsorption kinetics study was chosen according to the R^2 value. The PFO model was the

best alternative to describe the MB dye adsorption on ZnS-AHA NAs with R^2= (0.98-0.99) for all concentrations. The obtained results of adsorption kinetic modeling are reported in **Fig. 6** and **Table 1**. Adsorption rates (K_1) declined when the dye concentration increased because of the competition of dye molecules with the available adsorption active sites [42]. **Fig. 6** indicates that two different stages can be found in the kinetic profile. The first section of the curve corresponds to the diffusion of molecules on the NAs surface, which is generally the longest stage. The second stage corresponds to the adsorption equilibrium where the interaction between adsorbate and adsorbent surface takes place.

The adsorption capacity varied from 9.58 to 28.94 mg g^{-1}, when the dye concentration is increased from 10 to 50 mg/L, respectively. These values are close to the experimentally determined values from the adsorption isotherms. These high adsorption capacities are favored by the small particle size of ZnS-AHA NPs. The specific surface area of ZnS-AHA was found to be 36.82 cm^2 g^{-1}; this high specific surface area is a key factor to reaching these adsorption capacities, which also contributes to a fast mass transfer gradient for the MB diffusion to the NPs surface [24].

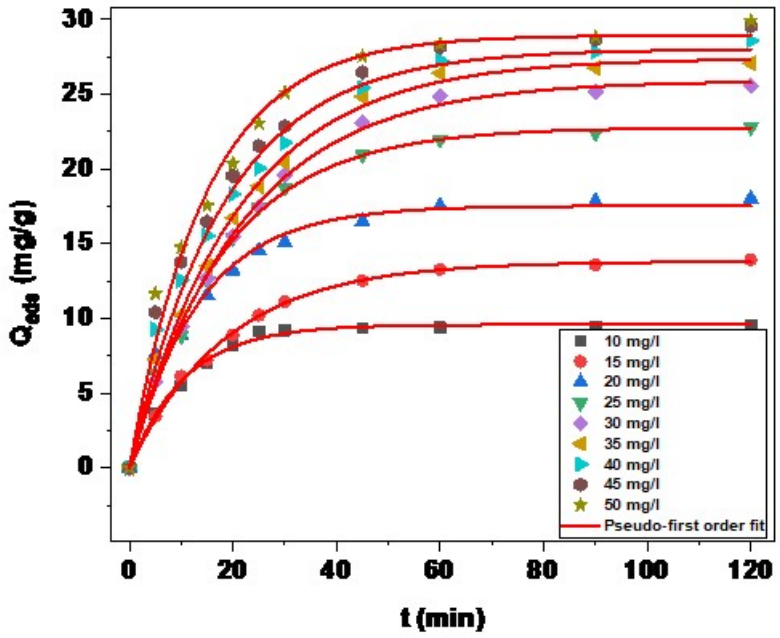

Fig.6: Modeling of MB adsorption kinetic using the pseudo-first order

Table 1: Pseudo-first-order kinetic parameters for the MB adsorption on ZnS-AHA NAs

Model	Pseudo-first order								
C(mg/l)	10	15	20	25	30	35	40	45	50
K1 (min^{-1})	0.09	0.05	0.08	0.05	0.04	0.05	0.05	0.06	0.07
qe (mg/g)	9.58	13.81	17.47	22.77	25.97	27.40	28.01	28.69	28.94

3.2.2. Dye adsorption isotherms

Adsorption isotherms are highly useful for understanding the mechanism of adsorption [43]. In general, adsorption isotherms provide information on the improvement of the adsorbents, a description of the affinity and the binding energy between adsorbate and adsorbent (whether or not there are lateral interactions between molecules), and the adsorption capacity [44]. The isotherm also gives information on mode adsorption (monolayer or multilayer adsorption).

In this study, the effect of the initial concentration of MB on the amount adsorbed (mg/g) by ZnS-AHA NPs was studied over a range of initial concentrations (10-50 mg/l) for MB. The adsorption isotherms assessed at room temperature of 298 K are shown in **Fig. 7**. According to Giles [45], the ZnS-AHA NPs adsorption isotherms show an L-form, indicating a relatively high affinity between the adsorbate and adsorbent. The maximum equilibrium adsorption capacity value is 29.92 mg/g.

The equilibrium data of MB onto ZnS NPs was examined using the most common Langmuir, Freundlich and Langmuir-Freundlich models to find out the suitable model that may be applied for the design and optimization of adsorption processes (see **Fig. 7** and ***Table 2***). The best applicable model of those is chosen from the coefficient R^2 value ($0 < R^2 < 1$). The Langmuir isotherm states that adsorption takes place with the monolayer formation of adsorbate molecules on a homogeneous adsorbent surface with uniform adsorption energies [46]. This model is very useful for the monomolecular adsorption of a solute by forming a single layer on the surface of an adsorbent; this model is used when the following conditions are met. The adsorbed species is fixed on a single well-defined site, and each site can fix a single adsorbed species, the adsorption energy of all sites is identical and independent of other species already adsorbed at neighboring sites. The following equation represents this model [24]:

$$q_e = q_{max} \frac{K_L C_e}{1+K_L C_e} \quad (3)$$

Where q_e is the equilibrium adsorption capacity (mg/mg), *Ce* (mg/L) is the dye concentration in solution at adsorption equilibrium, q_{max} (mg/g) is the maximum adsorption capacity of tested

nanoadsorbents and K_L (L/mg) is the Langmuir constant. On the other side, the Freundlich model implies an heterogeneous adsorption surface having sites with different adsorption energies. It is mostly applied to the heterogeneous solid catalysts and is a mathematical relation used to describe multilayer adsorption. It is described as [24]:

$$q_e = k_f C_e^{1/n_F} \quad (4)$$

where K_f(mg/g) is the Freundlich adsorption constant and n_F is the degree of nonlinearity between solution concentration and adsorption where, $1/n_F \in (0.1, 1)$ demonstrates favorable adsorption. In the end, the Langmuir -Freundlich (*L-F*) isotherm model is an equation based on the isotherms of Langmuir and Freundlich at the same time. It describes heterogeneous surfaces as well. The equation can be written as:

$$q_e = \frac{q_{max}(K_{LF}C_e)^{n_{LF}}}{1+(K_{LF}C_e)^{n_{LF}}} \quad (5)$$

where q_{max}(mg/g) is the maximum adsorption, the capacity of tested nano-adsorbents, K_{LF} is the adsorption affinity constant and n_{LF} is the heterogeneity index.

From the isothermal modeling results given in ***Table 2***,

We find that the Langmuir-Freundlich model better describes our experimental results, with q_{max}= 31.85 mg/g and R^2= 0.98. The Langmuir model shows that the surfaces of our samples are energy homogeneous and allow monomolecular adsorption of MB on our green NPs. On the other hand, Freundlich model n_F values are greater than 1 (n_F > 2.16) showing that adsorption is favorable and physical [42]. The maximum adsorption capacity calculated with the Langmuir-Freundlich model was 31.15 mg/g, which agreed with the experimental data of 29.92 mg/g and proves that the new robust green nano-adsorbents are good candidates for wastewater treatments.

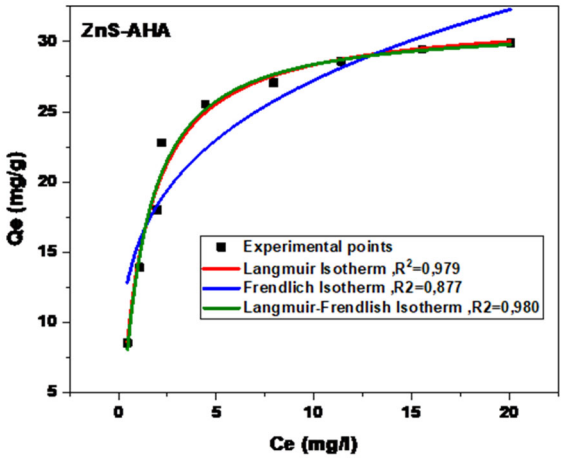

Fig. 7: The adsorption isotherms of MB dye using AHA-capped ZnS NPs.

Table 2: Parameters of the isotherm models for the MB adsorption on ZnS-AHA NPs

Langmuir isotherm (R^2 = 0.97)		
q_{max} (mg/g)	K_L	
31.8	0.80	
Freundlich isotherm (R^2 = 0.86)		
K_f (mg/g)	n_F	
15.52	2.41	
Langmuir-Freundlich (R^2 = 0.98)		
q_{max} (mg/g)	K_{L-F}	m
31.15	0.84	1.10

3.2.3. Statistical physics modeling

A statistical physics model was applied for MB supplement adsorption analysis via the calculation of the following physicochemical parameters: the number of the adsorbed dye molecules per adsorption site (n), the density of adsorption sites (D_M) and the corresponding adsorption energies. A monolayer advanced model was used to clarify the adsorption isotherms of MB on the tested ZnS-AHA NPs. This model considered that MB dye molecule formed a monolayer on NPs surface. The formation of the layer of adsorbed MB molecules resulted from the interactions between MB and NAs surface. This advanced model demonstrates that the main adsorption site in the green ZnS-AHA NPs could link a variable number of MB dye molecules (equal, inferior or superior to 1). This monolayer model is reported in equation 6 [24]:

$$q_e = \frac{nD_M}{1+\left(\frac{C_{\frac{1}{2}}}{C_e}\right)^n} \quad (6)$$

where $C_{1/2}$ is the concentration at half-saturation of MB on the ZnS-AHA NPs surface. Note that the calculation of adsorption energy via this model was performed with equation 6 [24]:

$$\Delta E^a{}_1 = R.T.\ln(\frac{C_s}{C_{1/2}}) \quad (7)$$

where C_s is the MB dye molecule solubility (i.e., 40 g/l), R is the universal ideal gas constant (8.314 x10^{-3} kJ K^{-1} mol^{-1}) and T (K) is the absolute value of adsorption temperature. The estimated values for model parameters are summarized in ***Table 3***, while the model fitting is given in **Fig. 8**. It is noted that the parameter n can be applied to describe the number of dye-adsorbed molecules per adsorption site and provides also details about the geometric adsorption position.

Geometrically, the position of an adsorbate can be described according to the number of molecules per adsorption site of the tested material.

Table 3 shows that n = (1.08-2.25) indicates that MB dye molecules could be linked or adsorbed via a non-parallel orientation or inclined, with a multimolecular adsorption process [8]. MB molecules can interact with the adsorbent surface thus forming an aggregation process where the formation of MB dimers in the solution and a multimolecular adsorption process ($n > 1$) could be expected on the prepared nano-adsorbents. This multimolecular adsorption phenomenon usually occurs for dye molecules. The density of adsorption sites D_M decreased with temperature from 28.73 to 11.45 mg g^{-1}. Indeed, if the number of adsorbed MB dye molecules per adsorption site increased, the space in the ZnS-AHA nanoparticles surface reduced and, consequently, the number of adsorption sites available for dye removal became limited [24]. Note that a high D_M value implies a high performance of the adsorbent because more adsorption sites are available for the adsorption of the target pollutant [8]. The adsorption capacities at saturation (Q_{sat}) decreased as a function of the aqueous solution temperature from 31.17 mg g^{-1} at 298 K to 25.49 mg g^{-1} at 318 K, thus indicating exothermic adsorption.

The last parameter to be analyzed is the adsorption energy**.** This adsorption energy is expressed as a function of the concentration at half-saturation and the solubility of MB dye in water (C_S). All the adsorption energies that characterize the interactions between MB molecules and ZnS-AHA nano-adsorbent surface were estimated by modeling the experimental data through the Hill model, and they are summarized in **Table 3**. It is observed that the adsorption energies ranged from 25.82 to 21.58 kJ mol^{-1}, suggesting the presence of physical interactions between MB dye molecules and the ZnS-AHA nano-adsorbent surface. It could be expected that weak electrostatic forces and hydrogen-bond interactions were involved in the adsorption of MB molecules on the functional groups of the green ZnS-AHA nanoparticles. When comparing the capacity of adsorption of ZnS-AHA to that of other previously published ZnS nanoparticles (Table 4), ZnS AHA presents higher capacity of adsorption, compared to naked ZnS NPs [47], to ZnS encapsulated with broccoli extract [48] and ZnS encapsulated with mercaptopropionic acid [24].

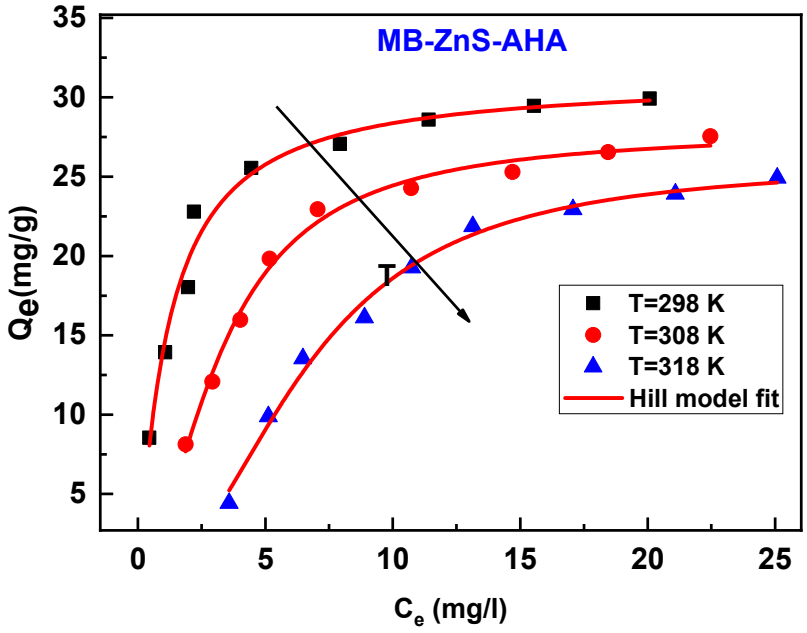

Fig. 8: Adsorption isotherm for statistical physics modeling of MB on ZnS-AHA.

Table 3: Parameters of the Hill model for the MB adsorption

T (K)	n	D_M (mg/g)	$C_{1/2}$ (mg/l)	Q_{sat} (mg/l)	ΔE_1^a (kJ/mol)
298	1.08	28.73	1.19	31.17	25.82
308	1.75	15.94	3.25	27.85	23.33
318	2.25	11.45	6.58	25.49	21.58

Table 4: Comparison of the adsorption capacity of various adsorbents with ZnS-AHA NPs towards MB dye.

Sr. No	**Sample**	**Dye**	**Time (min)**	**q_{max} (mg/g)**	**Ref. No**
1	ZnS-MPA	MB	120	25.18	[24]
2	ZnS	MB	120	15.65	[47]
3	ZnS-Broccoli	MB	60	9.00	[48]
9	ZnS-AHA	MB	120	31.85	Our work

3.3. Photocatalytic degradation of MB dye using ZnS-AHA NPs

3.3.1. Degradation pathways

In a process called "photocatalytic degradation of MB dye using sunlight irradiation," ZnS nanocatalysts are used to start a chemical reaction in the presence of sunlight. This reaction breaks down the dye molecule. The sunlight's irradiation plays a crucial role in this process by

providing the energy required for the photocatalytic reaction to occur. The energy from the sunlight excites the electrons in the photocatalyst material, which in turn react with the dye molecules to break them down. Preliminary experiments carried out with MB solution in the absence of the ZnS nano-catalysts reveal that less than 10 % of the dye was decomposed after 180 min of sunlight irradiation due to the OH* radicals coming from water or due to the self-sensitization light of dye molecules, proving that MB molecules present a good photostability. **Fig. 9** shows a series of UV-Vis absorption spectra for the methylene blue dye suspension in the presence of the AHA-capped ZnS NPs irradiated for 0, 10, 20, 30, 45, 60, 120 and 180 min. With increasing sunlight irradiation time, it was observed that a significant reduction in the absorption of the MB dye solution at the maximum peak at 664 nm was due to the break of the azo groups (C-S^{+}=C) bond responsible for the blue color which indicates the decomposition of the MB chromophoric structure [10].

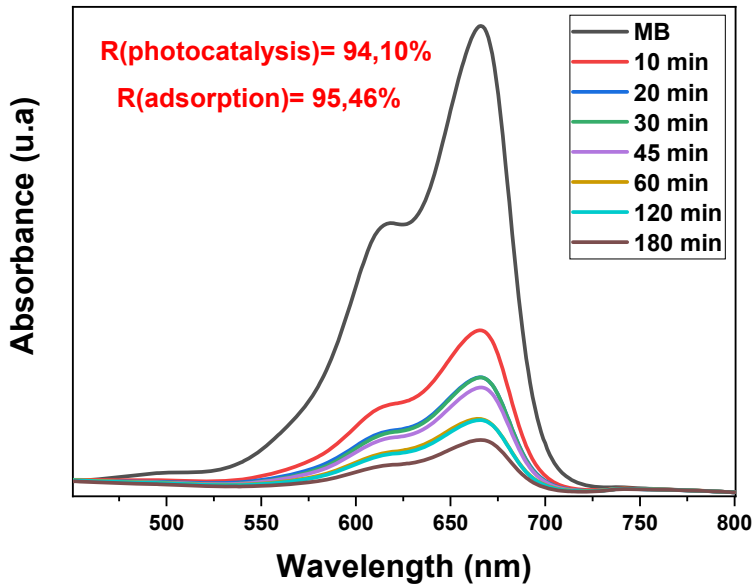

Fig. 9: Absorption spectral changes for the MB aqueous solution in the presence AHA capped ZnS NAs.

As a result, MB dye concentration decreased in the presence of the green ZnS-AHA NPs under sunlight irradiation until a full decolorization of the initial solution revealed that MB molecules were completely degraded. The degradation efficiency of AHA-capped ZnS NPs is given in **Table 5**. These results show a high degradation of MB dye using our synthesized NPs after 180 min of irradiation. We have recorded a rapid degradation of MB using the new plant extract-capped ZnS NPs leading to very effective decomposition in the first hour (89.18%). As a result,

the new green nano-adsorbents demonstrated a fast and powerful degradation (94.09%) and which makes them a promising and robust nanocatalyst for the dyes degradation. This high photodegradation activity can be explained by the reduction in electron-hole recombination [8]. In order to deduce kinetics from the degradation process, we calculated the effect of the irradiation time on the degradation using the normalized changes in the MB concentration (C/Co) and degradation efficiency (1- C/Co) for the nano-adsorbents represented in (**Fig. 10**). The intersection of these two curves indicated the half-life of the dye, which is the time reach to attend the MB half-concentration. The degradation performance is dependent on the high surface area of the crystal and morphology, which might enhance the number of photo-generated electron-hole pairs. Here, we suppose that *Artemisia Herba Alba* extract may influence the ZnS crystal growth with a high surface-to-volume ratio due to the small size of nanocrystals (4 nm) and subsequently high specific surface (36.82 cm^2 g^{-1}) which highly generate electron-hole pair at the conduction and valence band states under sunlight irradiation [30].In addition, another explanation is the ligand functional groups which is involved in the adsorption and the photocatalytic processes because *Artemisia Herba Alba* extract is plenty of phenol, proteins and flavonoids groups which include reactive hydroxyl radicals. These highly reactive hydroxyls and superoxide radicals formed by interaction with the charge carrier to the surface of the nanoparticles can react with MB dye adsorbed on ZnS leading to its degradation [49]. As a result, the probability of adsorption of MB molecules on the surface of ZnS NAs will be increased with the use of AHA. In order to calculate the rate constant (k) and half time for MB degradation, we have used **Eq.4** and **Fig. 10**; the summarized parameters are presented in ***Table 5***.

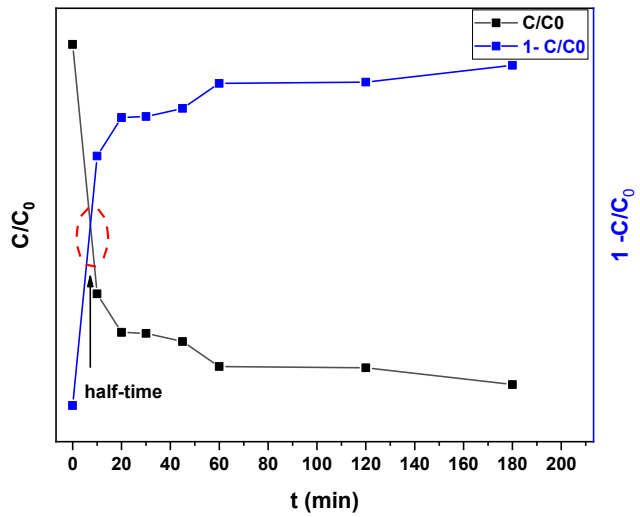

Fig. 10: C/Co curve and degradation efficiency (1-C/Co) for AHA capped ZnS NPs

Table 5: degradation efficiency of MB by ZnS-AHA NPs under sunlight irradiation.

t (min)	0 min	10 min	20 min	30 min	45 min	60 min	120 min	180 min
% Degradation of MB	0	69.27	79.81	79.90	82.27	89.18	89.63	94.09

The calculated rate constant (k) AHA-capped ZnS NPs was 0 0.012 min^{-1}. It is clear that the use of green ZnS-AHA nanocatalysts increases the photodegradation of the MB dye under sunlight which is confirmed by the small half-time value (7.41min). Finally, AHA-capped ZnS nanocatalysts showed a high photocatalytic performance due to the formation of NPs enriched with sulfur vacancies (Vs) and zinc interstitials (I_{Zn}) caused by stacking faults [24]. Therefore, as the plant extract-capped ZnS NPs present high defaults (dislocations, strain and stacking fault), this could facilitate the transfer of the photogenerated carriers by trapping the excited electrons and restraining the electron-hole recombination which increases the photocatalytic activity of these nano-adsorbents. This indicates that the ZnS capped with *Artemisia Herba Alba* groups can be considered as a promising photocatalyst that can operate under sunlight for the environmental removal of organic pollutants. Moreover, the green molecules of the plant extract are eco-friendly that making AHA-capped ZnS a good candidate for further applications (antibacterial activity and gas sensor). Some values of maximum quantities found in the photodegradation of MB on some other ZnS nanoparticles are presented in **Table 7**. ZnS-AHA presents the higher degradation efficiency, nevertheless, its degradation rate constant is lower than that of ZnS NPs coated with Acalypha indica extract [18] and that of ZnS NPs with cubic phase [53].

Table 6: Calculated parameters of photodegradation of MB in aqueous solution using ZnS-AHA NPs under sunlight irradiation.

Nanocatalyst	Degradation rate constant K (min^{-1})	Half-time $t_{1/2}$ (min)	Degradation efficiency η (%)
ZnS-AHA	0.012	7.41	94.09

Table 7: Comparison of the photocatalytic efficiency of various adsorbents with ZnS-AHA NPs towards MB dye.

Sr. No	Sample	Dye	Irradiation	Time (min)	Degradation rate constant *K* (min^{-1})	Degradation efficiency (%)	Ref. No
1	ZnS-TGA	MB	Sunlight	180	0.010	91.10	[10]
2	ZnS-CHI	MB	UV light	120	-------	87.00	[50]
3	ZnS-CC	MB	UV light	120	------	96.00	[51]
4	ZnS-S	MB	Visible light	180	------	81.00	[52]
5	ZnS-A	MB	UV light	180	0.071	93.00	[18]
6	ZnS	MB	Sunlight	180	0.013	87.38	[24]
7	ZnS	MB	Visible light	120	0.020	78.41	[53]
9	ZnS-AHA	MB	Sunlight	180	0.012	94.09	Our work

To help explain more about how photocatalysis works, Fig. 11 shows a possible photocatalytic mechanism for the degradation of MB dye by capped ZnS nanoparticles when exposed to sunlight.The first step is summarized by the adsorption phase of the dye molecules on the NAs surface. When the ZnS semiconductor was irradiated by sunlight with energy higher than the band gap, an electron (e^-)/ hole (h^+) pair was generated, where the electrons e^- will transfer from the valence band (VB) to the conduction band (CB) and the holes h^+ will be located in VB. The formed e^- and h^+ will migrate to the nano-adsorbent's surface and react with electronic reactants such as adsorbed O_2 to produce a superoxide anion radical ($\mathbf{O_2^{*-}}$). The photo-induced holes can be trapped to produce hydroxyl radical species ($\mathbf{OH^*}$), which are assumed to be the most essential and powerful oxidizing radicals for dye degradation. In addition, intrinsic defects in the crystal structure (i.e., Vs, and I_{Zn}) act as intermediate energy states for the electrons, inhibiting or delaying the rapid carrier recombination processes, which improve the separation of electron-hole pairs [54]. The active radical species (OH^* and O_2^{*-}) can effectively degrade dye molecules to form intermediates like propionic acid and malonic acid with the final products (CO_2 and H_2O) [55]. An analogous effect may be expected from the charged functional groups of the plant extract and the organic-capping agent at the nano-interfaces with ZnS under irradiation.

The main reactions that might be involved can be summarized as follows:

(a) Adsorption phase

$$\text{ZnS-AHA} + \text{MB} \rightarrow \text{ZnS-AHA-MB} \quad (18)$$

(b) (e^-)-(h^+) pair generation

$$ZnS\text{-}AHA + h\nu \rightarrow e_{BC}^{-} + h_{BV}^{+} \quad (19)$$

(c) Production of superoxide and hydroxyl radicals

$$e^{-} + O_2 \rightarrow O_2^{*-} \quad (20)$$

$$H_2O + h^{+} \rightarrow OH^{*} + H^{+} \quad (21)$$

$$h^{+} + OH^{-} \rightarrow OH^{*} \quad (22)$$

(d) Degradation phase

$$O_2^{*-} + C_{16}H_{18}ClN_3S \rightarrow \text{Intermediates} + CO_2 + H_2O \quad (23)$$

$$OH^{*} + C_{16}H_{18}ClN_3S \rightarrow \text{Intermediates} + CO_2 + H_2O \quad (24)$$

In the photocatalytic experiment to break down MB dye, it is clear that the hydroxyl radical is very important. To prove the effect of these species on the degradation process the photolysis experiments were carried out, which were based on sunlight irradiation without nanocatalysts. These preliminary experiments reveal that less than 10 % of dye was decomposed after 180 min of sunlight irradiation which demonstrates the importance of OH^{*} and $O2^{*-}$. These robust radicals found in high density in AHA-capped ZnS NPs arise from the phenol and flavonoid groups of the extract plant. The hydroxyl radical starts to attack dye molecules from the $C\text{-}S^{+}\text{=}C$ bond and other bonds to degrade the MB dye. According to the photocatalytic experiment, the biological and organic-capped ZnS nanoparticles show enhanced photocatalytic activity for the degradation of MB dye.

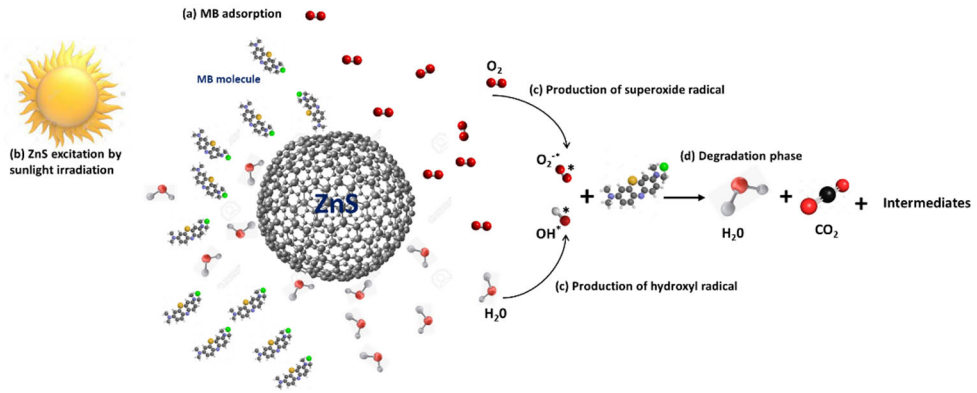

Fig. 11: Proposed MB dye degradation mechanism using capped-ZnS nano-adsorbents.

3.3.2. Recycling of the ZnS-AHA photocatalysts

Reusability studies are an important tool for evaluating the long-term viability of materials, and can help to take decisions about their use in a variety of applications. In this context, the photocatalytic stability of ZnS-AHA for MB degradation was thus studied. Repeatability experiments were conducted for 5 continuous cycles (**Fig.12**). After each run, the catalysts were collected and rinsed a few times with deionized water and ethanol, and dried at 100°C for 24 h before the beginning of the next cycle. Results reveal that the catalytic performance remains nearly unchanged and the degradation of MB is kept 92 ± 2 % after 5 successive cycles. These provide clear evidence of high physiochemical and photocatalytic stability of as-synthesized nanoparticles. We have added the following reusability studies in the photocatalytic section.

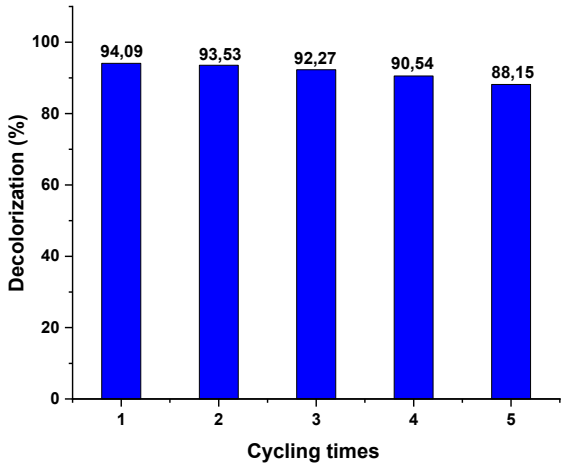

Fig. 12: Reusability of the ZnS-AHA nanocatalysts for the photodegradation of MB

6. Conclusion

In summary, the present findings demonstrate that AHA-capped ZnS NPs synthesized via a stable, simple and colloidal route at room temperature. An innovative green method for preparing luminescent ZnS nano-photocatalysts was developed, for the first time, using *Artemisia Herba Alba*. FTIR results confirmed the functionalization of nano-adsorbent surfaces by AHA. XRD analysis indicated the formation of nanocrystals with an almost pure cubic phase. The average size of AHA-capped ZnS nanocrystals calculated by using the Debye-Scherrer formula and observed by HR-TEM was 4 nm. The optical absorption spectra showed the appearance of an absorption edge shifted towards short wavelengths compared to that of the solid-state semiconductor ZnS. PL spectroscopy indicated that no significant emission intensity was observed which clearly revealed that AHA ligands could play the same role as organic ligands for use in

luminescence applications. Capped-ZnS NPs were used for MB removal under sunlight irradiation from an aqueous colloidal solution to investigate the adsorption-photocatalysis synergy. Results showed spontaneous exothermic adsorption with an adsorption capacity of up to 29.92 mg/g. Adsorption isotherms and statistical physics calculations were used to analyze the steric and energetic parameters associated with MB adsorption on the surface of nano-adsorbents. The green ZnS nanoparticles showed a remarkable sunlight photocatalytic activity for MB dye with a conversion rate of 89.18 % in the first hour. ZnS-AHA nanoparticles exhibited high adsorption and photocatalytic capacity indicating that new plant extracts are a promising capping agent for potential eco-friendly and environmental applications.

Acknowledgements

Region Auvergne Rhone-Alpes is acknowledged for the Pack Ambition International Project, EMBAI #246413. CNRS is acknowledged for the IRP NARES. Campus France is acknowledged for the financial support through PHC Maghreb EMBISALIM. S. OUNI thanks University of Monastir for providing the scholarship.

References

[1] R. Mia, M. Selim, A.M. Shamim, M. Chowdhury, S. Sultana, M. Armin, M. Hossain, R. Akter, S. Dey, H. Naznin, Review on various types of pollution problem in textile dyeing & printing industries of Bangladesh and recommandation for mitigation, J. Text. Eng. Fash. Technol. 5 (2019). https://doi.org/10.15406/jteft.2019.05.00205.

[2] L. Yu, Y. Luo, The adsorption mechanism of anionic and cationic dyes by Jerusalem artichoke stalk-based mesoporous activated carbon, J. Environ. Chem. Eng. 2 (2014) 220–229. https://doi.org/10.1016/j.jece.2013.12.016.

[3] A.K. Kushwaha, N. Gupta, M.C. Chattopadhyaya, Removal of cationic methylene blue and malachite green dyes from aqueous solution by waste materials of Daucus carota, J. Saudi Chem. Soc. 18 (2014) 200–207. https://doi.org/10.1016/j.jscs.2011.06.011.

[4] G. Pérez, P. Gómez, I. Ortiz, A. Urtiaga, Techno-economic assessment of a membrane-based wastewater reclamation process, Desalination. 522 (2022) 115409. https://doi.org/10.1016/j.desal.2021.115409.

[5] C. Liu, H. Mao, J. Zheng, S. Zhang, Tight ultrafiltration membrane: Preparation and characterization of thermally resistant carboxylated cardo poly (arylene ether ketone)s (PAEK-COOH) tight ultrafiltration membrane for dye removal, J. Membr. Sci. 530 (2017) 1–10. https://doi.org/10.1016/j.memsci.2017.02.005.

[6] C. Ding, M. Yi, B. Liu, C. Han, X. Yu, Y. Wang, Forward osmosis-extraction hybrid process for resource recovery from dye wastewater, J. Membr. Sci. 612 (2020) 118376. https://doi.org/10.1016/j.memsci.2020.118376.

[7] X. Li, L. Fu, F. Chen, S. Zhao, J. Zhu, C. Yin, Application of Heterogeneous Catalytic Ozonation in Wastewater Treatment: An Overview, Catalysts. 13 (2023) 342. https://doi.org/10.3390/catal13020342.

[8] N. Mohamed, S. Ouni, B. Mohamed, M. Bouzidi, A. Bonilla-Petriciolet, M. Haouari, Synthesis and preparation of acid capped CdSe nanocrystals as successful adsorbent and photocatalyst for the removal of dyes from water and its statistical physics analysis, Environ. Sci. Pollut. Res. (2022). https://doi.org/10.1007/s11356-022-20990-9.

[9] S. Ouni, N.B.H. Mohamed, N. Chaaben, A. Bonilla-Petriciolet, M. Haouari, Fast and effective catalytic degradation of an organic dye by eco-friendly capped ZnS and Mn-doped ZnS nanocrystals, Environ. Sci. Pollut. Res. 29 (2022) 33474–33494. https://doi.org/10.1007/s11356-021-17860-1.

[10] S. Ouni, N. Mohamed, M. Bouzidi, A. Bonilla-Petriciolet, M. Haouari, High impact of thiol capped ZnS nanocrystals on the degradation of single and binary aqueous solutions of industrial azo dyes under sunlight, J. Environ. Chem. Eng. 9 (2021) 105915. https://doi.org/10.1016/j.jece.2021.105915.

[11] B. Sarangi, S.P. Mishra, N. Behera, Advances in green synthesis of ZnS nanoparticles: An overview, Mater. Sci. Semicond. Process. 147 (2022) 106723. https://doi.org/10.1016/j.mssp.2022.106723.

[12] R. Chaudhary, K. Nawaz, A.K. Khan, C. Hano, B.H. Abbasi, S. Anjum, An Overview of the Algae-Mediated Biosynthesis of Nanoparticles and Their Biomedical Applications, Biomolecules. 10 (2020) 1498. https://doi.org/10.3390/biom10111498.

[13] F.C. Christopher, S.K. Ponnusamy, J.J. Ganesan, R. Ramamurthy, Investigating the prospects of bacterial biosurfactants for metal nanoparticle synthesis – a comprehensive review, IET Nanobiotechnol. 13 (2019) 243–249. https://doi.org/10.1049/iet-nbt.2018.5184.

[14] A. Yadav, K. Kon, G. Kratosova, N. Duran, A.P. Ingle, M. Rai, Fungi as an efficient mycosystem for the synthesis of metal nanoparticles: progress and key aspects of research, Biotechnol. Lett. 37 (2015) 2099–2120. https://doi.org/10.1007/s10529-015-1901-6.

[15] S. Munyai, L.M. Mahlaule-Glory, N.C. Hintsho-Mbita, Green synthesis of Zinc sulphide (ZnS) nanostructures using S. frutescences plant extract for photocatalytic degradation of dyes and antibiotics, Mater. Res. Express. 9 (2022) 015001. https://doi.org/10.1088/2053-1591/ac4409.

[16] A. El Nady, R.N. Abbas, N.M. Sorour, Biomediated nanosized ZnS using Ulva fasciata and Citrus japonica: A new bio-photocatalyst for textile wastewater treatment, Rendiconti Lincei Sci. Fis. E Nat. 33 (2022) 537–553. https://doi.org/10.1007/s12210-022-01076-7.

[17] H.R. Rajabi, F. Sajadiasl, H. Karimi, Z.M. Alvand, Green synthesis of zinc sulfide nanophotocatalysts using aqueous extract of Ficus Johannis plant for efficient photodegradation of some pollutants, J. Mater. Res. Technol. 9 (2020) 15638–15647. https://doi.org/10.1016/j.jmrt.2020.11.017.

[18] S. Kannan, N.P. Subiramaniyam, M. Sathishkumar, A novel green synthesis approach for improved photocatalytic activity and antibacterial properties of zinc sulfide nanoparticles using plant extract of Acalypha indica and Tridax procumbens, J. Mater. Sci. Mater. Electron. 31 (2020) 9846–9859. https://doi.org/10.1007/s10854-020-03529-x.

[19] S. Simon, N.R.S. Sibuyi, A.O. Fadaka, S. Meyer, J. Josephs, M.O. Onani, M. Meyer, A.M. Madiehe, Biomedical Applications of Plant Extract-Synthesized Silver Nanoparticles, Biomedicines. 10 (2022) 2792. https://doi.org/10.3390/biomedicines10112792.

[20] R. Belhattab, L. Amor, J.G. Barroso, L.G. Pedro, A. Cristina Figueiredo, Essential oil from Artemisia herba-alba Asso grown wild in Algeria: Variability assessment and comparison with an updated literature survey, Arab. J. Chem. 7 (2014) 243–251. https://doi.org/10.1016/j.arabjc.2012.04.042.

[21] H. Ekiert, M. Klimek-Szczykutowicz, A. Rzepiela, P. Klin, A. Szopa, Artemisia Species with High Biological Values as a Potential Source of Medicinal and Cosmetic Raw Materials, Molecules. 27 (2022) 6427. https://doi.org/10.3390/molecules27196427.

[22] M. Adoni, M. Yadam, S. Gaddam, R. Usha, V.S. Kotakadi, Antimicrobial, Antioxidant, and Dye Degradation Properties of Biosynthesized Silver Nanoparticles From Artemisia Annua L, Lett. Appl. NanoBioScience. 10 (2021) 1981–1992. https://doi.org/10.33263/LIANBS101.19811992.

[23] I. Khan, K. Saeed, I. Zekker, B. Zhang, A.H. Hendi, A. Ahmad, S. Ahmad, N. Zada, H. Ahmad, L.A. Shah, T. Shah, I. Khan, Review on Methylene Blue: Its Properties, Uses, Toxicity and Photodegradation, Water. 14 (2022) 242. https://doi.org/10.3390/w14020242.

[24] N. Bel Haj Mohamed, M. Bouzidi, S. Ouni, A.S. Alshammari, Z.R. Khan, M. Gandouzi, M. Mohamed, N. Chaaben, A. Bonilla-Petriciolet, M. Haouari, Statistical physics analysis of adsorption isotherms and photocatalysis activity of MPA coated CuInS2/ZnS nanocrystals for the removal of methyl blue from wastewaters, Inorg. Chem. Commun. 144 (2022) 109933. https://doi.org/10.1016/j.inoche.2022.109933.

[25] D. Amaranatha Reddy, C. Liu, R.P. Vijayalakshmi, B.K. Reddy (2014) Effect of Al doping on the structural, optical and photoluminescence properties of ZnS nanoparticles, J. Alloys Compd. 582: 257–264. https://doi.org/10.1016/j.jallcom.2013.08.051

[26] H. Asoufi, T. Al-Antary, A. Awwad (2018) biosynthesis and characterization of iron sulfide (FeS) nanoparticles and evaluation their aphicidal activity on the green peach aphid myzus persicae (Homoptera: aphididae), Fresenius Environ. Bull. 27: 7767–7775.

[27] Q.F. Nafa, S.M. Hussin, W.F. Hamadi (2021) Characterization of some active organic compound from Cold and Hot aqueous solvent and Study their Antibiotic of Artemisia herba-alba Asso plant oil, Egypt. J. Chem. 64: 6691–6709. https://doi.org/10.21608/ejchem.2021.72074.3587

[28] U.S. Senapati, D. Sarkar, Structural (2015) spectral and electrical properties of green synthesized ZnS nanoparticles using Elaeocarpus floribundus leaf extract, J. Mater. Sci. Mater. Electron. 26: 5783–5791. https://doi.org/10.1007/s10854-015-3137-6

[29] Y. Yu, L. Xu, J. Chen, H. Gao, S. Wang, J. Fang, S. Xu (2012) Hydrothermal synthesis of GSH–TGA co-capped CdTe quantum dots and their application in labeling colorectal cancer cells, Colloids Surf. B Biointerfaces. 95: 247–253. https://doi.org/10.1016/j.colsurfb.2012.03.011

[30] M. Jothibas, C. Manoharan, S. Johnson Jeyakumar, P. Praveen, I. Kartharinal Punithavathy, J. Prince Richard (2018) Synthesis and enhanced photocatalytic property of Ni doped ZnS nanoparticles, Sol. Energy. 159: 434–443. https://doi.org/10.1016/j.solener.2017.10.055

[31] V. Mote, Y. Purushotham, B. Dole (2012) Williamson-Hall analysis in estimation of lattice strain in nanometer-sized ZnO particles, J. Theor. Appl. Phys. 6: 6. https://doi.org/10.1186/2251-7235-6-6

[32] H. Matsumoto, T. Sakata, H. Mori, H. Yoneyama (1996) Preparation of Monodisperse CdS Nanocrystals by Size Selective Photocorrosion, J. Phys. Chem. 100: 13781–13785. https://doi.org/10.1021/jp960834x

[33] N. Ben Brahim, M. Poggi, N.B. Haj Mohamed, R. Ben Chaâbane, M. Haouari, M. Negrerie, H. Ben Ouada (2016) Synthesis, characterization and spectral temperature-dependence of thioglycerol-CdSe nanocrystals, J. Lumin. 177: 402–408. https://doi.org/10.1016/j.jlumin.2016.05.026

[34] Y. Piña-Pérez, O. Aguilar-Martínez, P. Acevedo-Peña, C.E. Santolalla-Vargas, S. Oros-Ruíz, F. Galindo-Hernández, R. Gómez, F. Tzompantzi (2018) Novel ZnS-ZnO composite synthesized by the solvothermal method through the partial sulfidation of ZnO for H2 production without sacrificial agent, Appl. Catal. B Environ. 230: 125–134. https://doi.org/10.1016/j.apcatb.2018.02.047

[35] P.K. Jaseela, J. Garvasis, A. Joseph (2019) Selective adsorption of methylene blue (MB) dye from aqueous mixture of MB and methyl orange (MO) using mesoporous titania (TiO2) – poly vinyl alcohol (PVA) nanocomposite, J. Mol. Liq. 286: 110908. https://doi.org/10.1016/j.molliq.2019.110908

[36] B.H. Hameed (2009) Evaluation of papaya seeds as a novel non-conventional low-cost adsorbent for removal of methylene blue, J. Hazard. Mater. 162: 939–944. https://doi.org/10.1016/j.jhazmat.2008.05.120

[37] M. Arshadi, F. SalimiVahid, J.W.L. Salvacion, M. Soleymanzadeh (2014) Adsorption studies of methyl orange on an immobilized Mn-nanoparticle: kinetic and thermodynamic, RSC Adv. 4: 16005–16017. https://doi.org/10.1039/C3RA47756H

[38] M. Ghaedi, H. Hossainian, M. Montazerozohori, A. Shokrollahi, F. Shojaipour, M. Soylak, M.K. Purkait (2011) novel acorn-based adsorbent for the removal of brilliant green, Desalination. 281: 226-233. https://doi.org/10.1016/j.desal.2011.07.068

[39] Y. Bulut, H. Aydın (2006) A kinetics and thermodynamics study of methylene blue adsorption on wheat shells, Desalination. 194: 259–267. https://doi.org/10.1016/j.desal.2005.10.032

[40] H. Khojasteh, M. Salavati-Niasari, A. Abbasi, F. Azizi, M. Enhessari, Synthesis (2016) characterization and photocatalytic activity of PdO/TiO2 and Pd/TiO2 nanocomposites, J. Mater. Sci. Mater. Electron. 27: 1261–1269. https://doi.org/10.1007/s10854-015-3884-4

[41] M. Ghasemi, N. Ghasemi, G. Zahedi, S.R.W. Alwi, M. Goodarzi, H. Javadian (2014) Kinetic and equilibrium study of Ni(II) sorption from aqueous solutions onto Peganum harmala-L, Int. J. Environ. Sci. Technol. 11: 1835–1844. https://doi.org/10.1007/s13762-014-0617-9

[42] S. Dawood, T.K. Sen (2012) Removal of anionic dye Congo red from aqueous solution by raw pine and acid-treated pine cone powder as adsorbent: Equilibrium, thermodynamic, kinetics, mechanism and process design, Water Res. 46: 1933–1946. https://doi.org/10.1016/j.watres.2012.01.009

[43] P. Luo, Y. Zhao, B. Zhang, J. Liu, Y. Yang, J. Liu (2010) Study on the adsorption of Neutral Red from aqueous solution onto halloysite nanotubes, Water Res. 44: 1489–1497. https://doi.org/10.1016/j.watres.2009.10.042

[44] Q. Hu, Z. Xu, S. Qiao, F. Haghseresht, M. Wilson, G.Q. Lu (2007) A novel color removal adsorbent from heterocoagulation of cationic and anionic clays, J. Colloid Interface Sci. 308: 191–199. https://doi.org/10.1016/j.jcis.2006.12.052

[45] C.H. Giles, D. Smith, A. Huitson (1974) A general treatment and classification of the solute adsorption isotherm. I. Theoretical, J. Colloid Interface Sci. 47: 755–765. https://doi.org/10.1016/0021-9797(74)90252-5

[46] I. Langmuir (1918) The adsorption of gases on plane surfaces of glass, mica and platinum, J. Am. Chem. Soc. 40, 1361-1403. https://doi.org/10.1021/ja02242a004

[47] X. Liu,X. Zhang, Y. Liu,M. Liu,X. Miao,Y. Wang (2022) Influence of ZnS crystal morphology on adsorption-photocatalytic efficiency of pseudocrystal ZnS nanomaterials for methylene blue degradation, J. Mol. Struct.1256:132514-132524. https://doi.org/10.1016/j.molstruc.2022.132514

[48] A. Q. Abed , A. M. Al Hindawi , H. F. Alesary (2022) Green Synthesis of Zinc Sulfide Nanoparticles for the Removal of Methylene Blue Dye from Aqueous Solution, NanoWorld J.8:79-84. http://doi.org/10.17756/nwj.2022-103.

[49] C. Lu, C. Liu, R. Chen, X. Fang, K. Xu, D. Meng (2016) Synthesis and characterization of ZnO/ZnS/CuS ternary nanocomposites as high efficient photocatalyst in visible light, J. Mater. Sci. Mater. Electron. 27: 6947–6954. https://doi.org/10.1007/s10854-016-4649-4

[50] A. A.P. Mansura, H. S. Mansura, F. P. Ramanerya, L. Carlos Oliveirab, P. P. Souza (2014) “Green” colloidal ZnS quantum dots/chitosan nano-photocatalysts for advanced oxidation processes: Study of the photodegradation oforganic dye pollutants, Appl. Catal. 158–159 (2014) 269–279. https://doi.org/10.1016/j.apcatb.2014.04.026

[51] J. Chen, B. Hu, J. Zhi (2015) Optical and photocatalytic properties of Corymbia citriodora leaf extract synthesized ZnS nanoparticles, Physica E Low Dimens. Syst. 79 :103-106. https://doi.org/10.1016/j.physe.2015.12.015

[52] S. k. Mani, S. Manickam, V. Muthusamy, R. Thangaraj (2018) Antimicrobial Activity and Photocatalytic Degradation Properties of Zinc Sulfide Nanoparticles Synthesized by Using Plant Extracts, J Nanostruct 8(2): 107-118.

[53] Z. Ye, L. Kong, F. Chen, Z. Chen, Y. Lin, C. Liu (2018) A comparative study of photocatalytic activity of ZnS photocatalyst for degradation of various dyes, Optik. 164: 345–354. https://doi.org/10.1016/j.ijleo.2018.03.030

[54] A.A.P. Mansur, H.S. Mansur, F.P. Ramanery, L.C. Oliveira, P.P. Souza (2014) “Green” colloidal ZnS quantum dots/chitosan nano-photocatalysts for advanced oxidation processes: Study of the photodegradation of organic dye pollutants, Appl. Catal. B Environ. 158–159: 269–279. https://doi.org/10.1016/j.apcatb.2014.04.026

[55] J. Lin, Z. Luo, J. Liu, P. Li (2018) Photocatalytic degradation of methylene blue in aqueous solution by using ZnO-SnO2 nanocomposites, Mater. Sci. Semicond. Process. 87: 24–31. https://doi.org/10.1016/j.mssp.2018.07.003

Supplementary Information

A novel green synthesis of zinc sulfide nanoparticles using *Artemisia Herba Alba* plant extract for adsorption and photocatalysis of methyl blue dye

2. Experimental details

Chemicals and reagents together with Artemisia Herba Alba plant extraction were demonstrated in the first section of the Supplementary Materials.

2.1. Chemicals and Reagents

Analytical-grade chemicals were used from commercial sources without any further purification. Zinc (II) acetate dihydrate (Zn $[CH_3COO]_2.2H_2O \geq 98\%$), sodium sulfide ($Na_2S \geq 98\%$), and methylene blue dye ($C_{16}H_{18}ClN_3S$ ≥50%, MW = 319,85 g/mol) were purchased from Sigma-Aldrich. Ultra-pure water (UPW) from the Millipore system was employed in all aqueous solutions (resistivity > 18 MOhm.com).

2.2. *Artemisia Herba Alba* extraction

Artemisia Herba Alba (AHA) plants were collected from Tunisia. The selected leaves of AHA plants were washed with deionized water and then dried in the shade at room temperature and ground into powder. 11.5 g of powder was added to 200 mL of distilled water. The mixtures were boiled at 100 °C for 2h and filtered at room temperature. The filtered aqueous solution constitutes the extract of *A. herba alba*, which was used for ZnS nanoparticle fabrication in the present study. **Fig. S1** shows a picture of *A. herba alba* leaves and their extract.

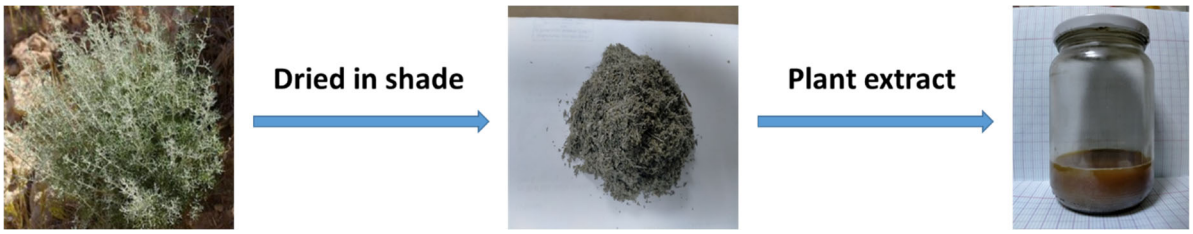

Fig.S1: *Artemisia Herba Alba* plant and its extract.

2.3. Synthesis of ZnS nanoparticles

The colloidal wet chemical route has been used to describe in detail how ZnS nanoparticles are made [1]. The green synthesis of the ZnS NPs was carried out employing *Artemisia Herba Alba* (AHA) extract as a complexing agent. In the typical synthesis process of AHA-capped ZnS NPs, 20 ml of AHA aqueous extract was mixed with 3 mM of $Zn[OOCCH_3]_2 \cdot 2H_2O$ solution

(50 ml). The mixture was then agitated and degassed in the presence of N_2 for 30 min. In a second step, under stirring, 1.2 mM of Na_2S solution (30 ml) was added to the solution containing Zn-AHA complexes at room temperature. Then, the mixture was heated under N_2 reflux at 100 °C for 3 h to obtain AHA-capped ZnS NPs. The final solution was to allow the solution to cool down naturally at room temperature to stop the growth of NPs. The nanoparticle powder was separated by centrifugation for 20 min and washed with water and ethanol, and then it was stored at room temperature to be used later in dye removal studies.

2.4. Adsorbent characterization

Numerous techniques were used to characterize AHA-capped ZnS NPs. XRD measurements were carried out using a Panalytical X' Pert Pro diffractometer with a CuKα radiation source (λ=1,542Å). Fourier transform infrared (FTIR) spectra were obtained in the transmission mode using a Perkin Elmer version 5.3 spectrophotometer in the spectral range of 400–4000 cm^{-1} at room temperature using KBr pellet disks. High-resolution transmission electron microscopy (HR-TEM) images were recorded using a JEM-2100 microscope operating at 200 kV and equipped with an Energy Dispersive X-ray (EDX) system for element chemical analysis. A drop of nanocrystal solution was poured onto carbon-coated copper grids to obtain HR-TEM samples, where the excess solvent was evaporated. The nanocrystal size and size-distribution data were collected based on the HR-TEM images by measuring at least 100 randomly selected nanocrystals using an image processing program (ImageJ, version 1.50). Absorbance spectra were registered using a SPECORD 210 Plus spectrophotometer in the range of 200–800 nm at room temperature with a quartz cuvette. Photoluminescence (PL) spectroscopy was used to study the defects and emission properties of the ZnS NAs using a helium-cadmium laser as an exciting source of 325 nm.

2.5. Dye adsorption experiments

The process of molecules or particles sticking to the surface of a material or substrate is called adsorption. The study of the adsorption of MB onto AHA capped ZnS nanoparticles involves investigating the interaction between the dye and the surface of the nanoparticles. This can be done by preparing a suspension of the nanoparticles and adding a known concentration of MB to it. After stirring and allowing the suspension to equilibrate for a period of time, the concentration of MB remaining in the solution is measured using a UV-Vis spectrophotometer (SPECORD 210 Plus, Tunisia). All adsorption tests were performed with magnetic stirring in the dark.

You can figure out how well the nanoparticles absorb by figuring out the difference between how much MB was in the solution at the beginning and how much was left at the end. This information can be used to figure out how well the nanoparticles remove MB from the water. Factors that can affect the adsorption of MB on AHA capped ZnS nanoparticles include the concentration of MB, the pH of the solution, the temperature, and the size and surface area of the nanoparticles. These parameters can be varied to optimize the adsorption capacity of the nanoparticles. To check the effect of these parameters, each one was tested individually by holding all the other variables fixed. Contact time (0-120 min), initial concentrations of MB (10-30 mg/l), adsorbent dose (0.1-2 g/l), different medium pH (5-9) and temperature range (298-318 K) were studied to find the effect of these variables on the adsorption operation of ZnS nanoparticles in aqueous solutions. The MB adsorbed amount Qe (mg/g) as well as the percent dye removal efficiency (%) by the ZnS NPs can be expressed as [2]:

$$Q_e = \frac{(C_0 - C_e)V}{m} \quad (1)$$

$$Dye\ Adsorption\ efficiency\ (\%) = \frac{(C_0 - C_e)}{C_0} x\ 100 \quad (2)$$

where C_0 and C_e is the initial and the equilibrium concentrations of dye in the solution, in (mg/L), respectively, V is the volume of the MB solution in (mL), and m is the mass of the ZnS-AHA in (mg). The plot of equilibrium adsorption capacity Q_e against equilibrium concentration C_e in the liquid phase is graphically illustrated to determine the equilibrium isotherm.

Furthermore, the density ρ was calculated using the following expression [2]:

$$\rho = \frac{ZM}{N_A V} \quad (3)$$

Where Z is the number of atoms per unit cell, M (g mol^{-1}) is the molecular weight of the ZnS, V is the volume of the unit cell (cm^{-3}) and N_A is the Avogadro number. The specific surface area S (cm^2 g^{-1}) of ZnS nano-particles was calculated using the next equation [2]:

$$S = \frac{6}{\rho D} \quad (4)$$

Where ρ (g cm^{-1}) and D (nm) are the x-ray density of cubic or hexagonal nano-particles and the average particle size, respectively.

2.6. Photocatalytic degradation measurements

The photocatalytic performance of ZnS-AHA NPs was measured by the photodegradation of MB as model dye. The photocatalytic experiments were carried out at 300 K and pH 7 with the

initial concentration and volume of 10 mg/l and 20 ml respectively in the presence of 20 mg ZnS NAs. At midday on a clear day in Tunisia, the intensity of sunlight at the Earth's surface is typically around 1000 watts per square meter (W/m²). By contrast to sunlight, UV radiation represented only 5% (50 Wm^{-2}) of the total available solar flux received at the surface of the earth in the most favorable sunlight conditions [1]. After the adsorption phase (in the dark), the suspensions were submitted to sunlight irradiation between 11 am and 2 pm to rate the dye degradation. The photocatalytic activity was examined by monitoring the concentration in samples of 2 mL of the preparation suspension taken after filtration at different irradiation periods (0, 10, 20, 30, 45, 60, 120, 180 min). According to the Beer-Lambert law, the degradation performance was evaluated by measuring the optical absorption at the maximum absorption wavelength of MB at 664 [2]. The degradation efficiency and rate were calculated using the following equations [2]:

$$\eta = \frac{C_0 - C_t}{C_0} \text{ x } 100 \quad (5)$$

$$kt = Ln\left(\frac{C_0}{C_t}\right) \quad (6)$$

$$t_{1/2} = \frac{Ln(2)}{K} \quad (7)$$

Where $C_0, C,$ are the concentrations (mg/L) and A_0 and A are the absorbances of MB dye solution before and after irradiation, respectively, at different times using the NPs. Note that K (min^{-1}) is the apparent reaction rate constant, which is calculated from of Ln (C/C_0) or Ln (A/A_0) versus t.

3. Results and discussion

3.1. ZnS-AHA Nanoparticles characterization

The FTIR spectrometer was used to measure the vibrational frequencies of bonds in the molecules and to confirm the presence of different functional groups on the surface of ZnS nanoparticles (**Fig. S2**). The absorption band at 540 cm^{-1} was observed due to the Zn-S stretching vibrations [3]. The presence of Zn-S vibration clearly indicated that ZnS NPs was successfully formed. Absorption peak was observed at 3319 cm^{-1} which is due to the alcohol/phenol group (-OH) stretching vibration [4]. The strong broad peak at 3665 cm^{-1} is attributed to N-H stretching mode of the secondary amides coming particularly from the identified molecule dihydroxanthin of plant extract [5]. The peak at 2978 cm^{-1} is probably ascribed to C-H alkane stretching, while the band at 2893 cm^{-1} could be assigned to the C–H stretching branched alkene,

particularly from the identified molecule cis-hydroxydavanone compound of AHA extract [5]. The peak at 1575 cm^{-1} could be due to C=O carbonyl stretching group and the peak at 1057 cm^{-1} was assigned to the stretching vibrations of primary alcohol groups in the AHA extracts [6]. Hence, these two peaks confirmed the presence of flavonoids or polyphenolic compounds in AHA-capped ZnS NPs [6]. The peaks at 1393 and 1259 cm^{-1} corresponded to CH_3 and C-O stretching vibration coming mainly from the identified molecule vulgarin [5]. FTIR analysis evidenced that green nanoparticles were stabilized with the major phytoconstituents of AHA extract.

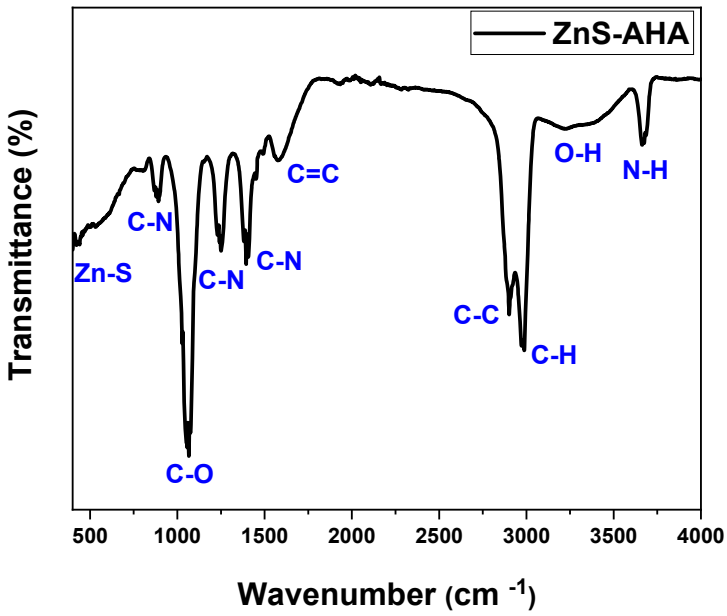

Fig. S2: FTIR spectrum of AHA-capped ZnS nanoparticles.

The crystal structures of the as-synthesized ZnS nanoparticles prepared using AHA as a capping agent was studied by X-ray diffraction (XRD) and the obtained XRD patterns are shown in **Fig. S3**. The diffraction peaks are broadly confirming the nanometric size of the ZnS particles. For the phase identification, diffraction patterns of the ZnS were compared and analyzed using the diffraction standards of the wurtzite phase (JCPDS card No.80-0020) and zinc blend phase (JCPDS card No.80-0007). XRD patterns can be indexed as cubic zinc blende structure, and they appear in good agreement with JCPDS data card No. 80-0007 with prominent peaks corresponding to the reflections at (111) (220) and (311) planes. The non-appearance of diffrac-

tion peaks related to the wurtzite phase demonstrates that AHA capping favors the cubic structure. To better quantify the effect of the stabilizers, the size of the nanoparticles was estimated using the Scherrer formula [7]:

$$D = \frac{K\lambda}{\beta \cos(\theta)} \quad \text{(S.1)}$$

Where D is the average crystallite size (Å), $k = 0.9$ is the Scherrer constant, λ is the wavelength of X-ray (1.5402 Å) Cu Kα radiation, β is the full width at half maximum of the diffraction peak (in radian) and θ is the Bragg diffraction angle, respectively. The estimated average size of the ZnS-AHA nanocrystals was found to be nearly equal to 4 nm. The smaller size of the ZnS crystallites encapsulated by AHA extract is most likely due to the strong interaction of AHA molecules with ZnS nanocrystals which makes the growth slower [8]. On the other hand, the lattice constant of the cubic phase of ZnS nanocrystals can be estimated using the following expressions:

$$d_{hkl}^2 = \frac{a_c^2}{h^2+k^2+l^2} \quad \text{(S.2)}$$

Where d_{hkl} is the inter-reticular distance for the cubic structure; h, k, and l are Miller indices; λ is the wavelength of the X-ray radiation; a_c, *is* the lattice constant of the cubic phase of ZnS nanocrystals. The calculated average value of the lattice and the inter-reticular distance parameters of AHA ZnS nanocrystals was a= 5.4 Å and d_{hkl}=0.31 nm. It should be kept in mind that the Scherrer formula considers only the size effects coming from the diffraction results, and it then offers a lower limit for the nanocrystals size and neglects the micro-strain [9].

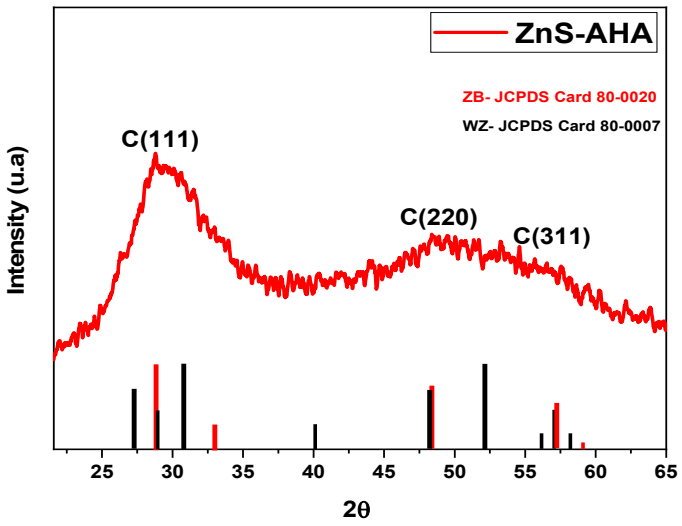

Fig. S3: DRX patterns of AHA-capped ZnS nanocrystals.

Figure S4a shows the HR-TEM images of the AHA-capped ZnS NPs, which are round, and a histogram of their sizes. Their aggregation could be due to the high concentration of nanoparticles. The histogram of nanocrystal size distribution shows that the average crystal size is 4.3 ± 0.5 nm. These results are in good agreement with the XRD results. The d-spacing determined from the digital micrograph for ZnS is 0.30 nm, which is close to the spacing of (111) diffraction plane of the cubic phase [2]. Comparing the values calculated by Bragg law, it is evident that the growth of ZnS-AHA occurs preferentially along the direction [111]. NPs elemental composition was determined by EDX (**Fig. S4b**). Zn and S are the major elemental components. The presence of C is related to the TEM grid and other peaks, Si and P, are probably due to residues coming from the synthesis and the grid.

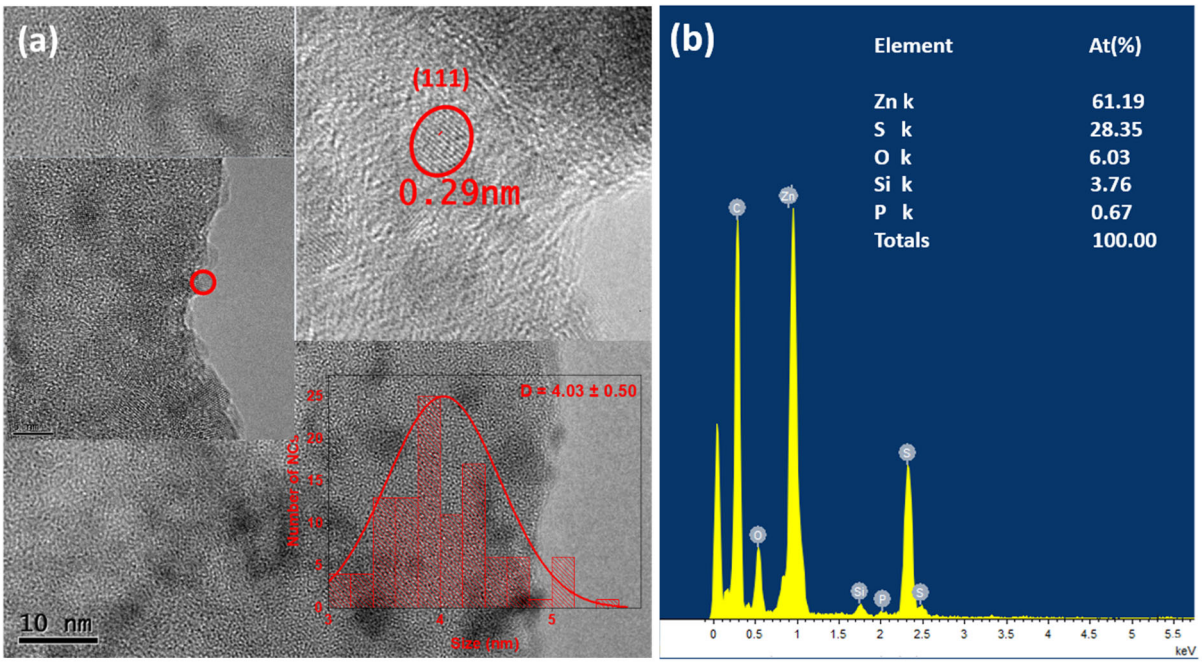

Fig. S4: (a) HR-TEM images of ZnS-AHA nanocrystals with an inset showing the 0.29 nm lattice spacing that corresponded to the (111) plane and (b) EDX results.

3.1.2. Optical study of ZnS-AHA NPs

In order to investigate the optical properties and the impact of ligand on the stability and size distribution of the nanoparticles, the optical absorption spectra of the ZnS NAs dispersed in water were recorded in (**Fig. S5**). The UV-Visible absorption spectrum of ZnS NAs suspension shows an absorption band at 325 nm related to the first electronic transition $1S_e$-$1S_h$ [10]. The blue shift compared to bulk ZnS (344 nm, E_g = 3.6 eV) is due to the quantum confinement of charge carriers due to the small particle size. This tendency is characteristic of semiconductors

II-VI, mainly associated with the nanocrystal size distribution and sub-bandgap transitions arising from the intrinsic-extrinsic defect states. We have determined graphically the value of the optical and band-gap energy *Eg* using the following Tauc relation [11]:

$\alpha h\nu =$

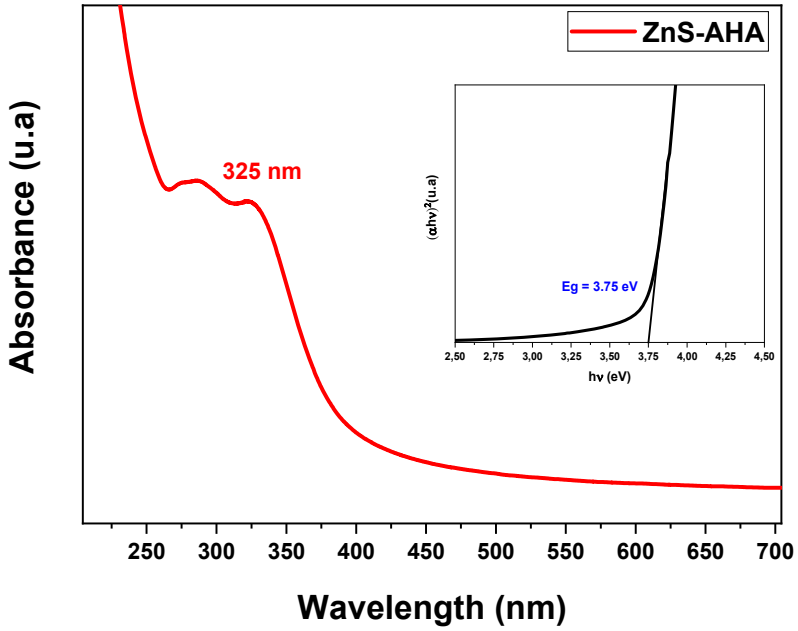

$$A\ (h\nu - Eg)^n \qquad \text{(S.3)}$$

Here, α is the absorption coefficient, A is a constant, h is the Planck constant, ν is the frequency of radiated photons and n is a transition-dependent factor (n = 1/2 for direct semiconductors). The optical gap energy of the capped ZnS NPs is obtained by extrapolating the plot of the function $(\alpha h\nu)^2$ to the value $\alpha = 0$. The intersection of the line with the horizontal axis gives the band gap energy value, (see insert in **Fig. S5**). The estimated band gap energy for the green ZnS is 3.70 eV. It is clear that the gap energy of these ZnS NPs shifts towards the blue, compared to that of the bulk ZnS (E_g = 3.6 eV); this is due to the very small size of NPs, which induces a quantum confinement effect (QCE) [12].

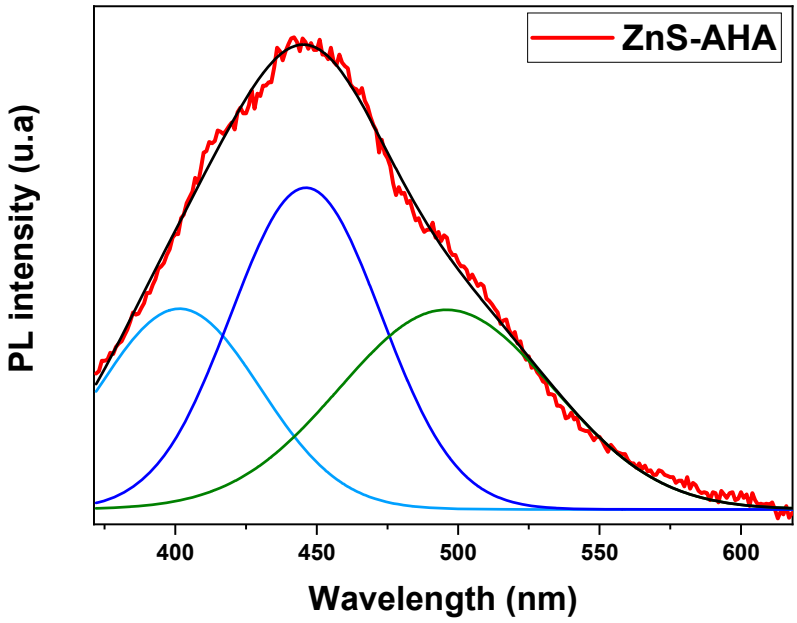

Fig. S5: Absorption spectra for ZnS nanoparticles prepared with AHA plant extract. The determination of the energy band gap using Tauc Relation is shown in the inset.

Fig. S6 shows the emission spectra of ZnS NPs obtained with an excitation wavelength λ_{exc}= 325 nm at room temperature. An intense and wide band centered at 450 nm dominates the spectrum. The emission spectra are deconvoluted using three Gaussian profiles associated with three main bands. The first band is less intense and has a spectral width of a few nm and is strongly correlated with the size of the nanoparticles. This band was attributed to the direct band-to-band recombination of excitons. The second emission band in the blue region (450 nm), which dominates the spectrum, was attributed to recombination between electrons and holes at the edges of conduction and valence bands respectively, or involves very shallow recombination centers (sulfur vacancies Vs) [13]. Finally, the green emission band (500 nm) was attributed to the interstitial zinc atom (I_{Zn}) [14]. The FWHM of the main emission band is equal to 62 nm which is related to the size dispersion of the ZnS-AHA NPs.

Fig. S6: Gaussian adjustment of PL spectra of AHA capped ZnS NPs.

References

[1] S. Ouni, N. Mohamed, M. Bouzidi, A. Bonilla-Petriciolet, M. Haouari, High impact of thiol capped ZnS nanocrystals on the degradation of single and binary aqueous solutions of industrial azo dyes under sunlight, J. Environ. Chem. Eng. 9 (2021) 105915. https://doi.org/10.1016/j.jece.2021.105915.

[2] N. Mohamed, S. Ouni, B. Mohamed, M. Bouzidi, A. Bonilla-Petriciolet, M. Haouari, Synthesis and preparation of acid capped CdSe nanocrystals as successful adsorbent and photocatalyst for the removal of dyes from water and its statistical physics analysis, Environ. Sci. Pollut. Res. (2022). https://doi.org/10.1007/s11356-022-20990-9.

[3] D. Amaranatha Reddy, C. Liu, R.P. Vijayalakshmi, B.K. Reddy (2014) Effect of Al doping on the structural, optical and photoluminescence properties of ZnS nanoparticles, J. Alloys Compd. 582: 257–264.

[4] H. Asoufi, T. Al-Antary, A. Awwad (2018) biosynthesis and characterization of iron sulfide (FeS) nanoparticles and evaluation their aphicidal activity on the green peach aphid myzus persicae (Homoptera: aphididae), Fresenius Environ. Bull. 27: 7767–7775.

[5] Q.F. Nafa, S.M. Hussin, W.F. Hamadi (2021) Characterization of some active organic compound from Cold and Hot aqueous solvent and Study their Antibiotic of Artemisia herba-alba Asso plant oil, Egypt. J. Chem. 64: 6691–6709.

[6] U.S. Senapati, D. Sarkar, Structural (2015) spectral and electrical properties of green synthesized ZnS nanoparticles using Elaeocarpus floribundus leaf extract, J. Mater. Sci. Mater. Electron. 26: 5783–5791.

[7] M. Adoni, M. Yadam, S. Gaddam, R. Usha, V.S. Kotakadi, Antimicrobial, Antioxidant, and Dye Degradation Properties of Biosynthesized Silver Nanoparticles From Artemisia Annua L, Lett. Appl. NanoBioScience. 10 (2021) 1981–1992. https://doi.org/10.33263/LIANBS101.19811992.

[8] Y. Yu, L. Xu, J. Chen, H. Gao, S. Wang, J. Fang, S. Xu (2012) Hydrothermal synthesis of GSH–TGA co-capped CdTe quantum dots and their application in labeling colorectal cancer cells, Colloids Surf. B Biointerfaces. 95: 247–253.

[9] M. Jothibas, C. Manoharan, S. Johnson Jeyakumar, P. Praveen, I. Kartharinal Punithavathy, J. Prince Richard (2018) Synthesis and enhanced photocatalytic property of Ni doped ZnS nanoparticles, Sol. Energy. 159: 434–443.

[10] V. Mote, Y. Purushotham, B. Dole (2012) Williamson-Hall analysis in estimation of lattice strain in nanometer-sized ZnO particles, J. Theor. Appl. Phys. 6: 6.

[11] H. Matsumoto, T. Sakata, H. Mori, H. Yoneyama (1996) Preparation of Monodisperse CdS Nanocrystals by Size Selective Photocorrosion, J. Phys. Chem. 100: 13781–13785.

[12] L. Meng, A. Maçarico, R. Martins (1995) Study of annealed indium tin oxide films prepared by rf reactive magnetron sputtering, vacuum. 46: 673–680.

[13] N. Ben Brahim, M. Poggi, N.B. Haj Mohamed, R. Ben Chaâbane, M. Haouari, M. Negrerie, H. Ben Ouada (2016) Synthesis, characterization and spectral temperature-dependence of thioglycerol-CdSe nanocrystals, J. Lumin. 177: 402–408.

[14] Y. Piña-Pérez, O. Aguilar-Martínez, P. Acevedo-Peña, C.E. Santolalla-Vargas, S. Oros-Ruíz, F. Galindo-Hernández, R. Gómez, F. Tzompantzi (2018) Novel ZnS-ZnO composite synthesized by the solvothermal method through the partial sulfidation of ZnO for H2 production without sacrificial agent, Appl. Catal. B Environ. 230: 125–134.